RAPID, TIME-RESOLVED PROXIMITY LABELING BY SBP1 IDENTIFIES A PORIN DOMAIN PROTEIN AT THE MALARIA PARASITE PERIPHERY

David Anaguano[1,2], Carrie F. Brooks[2], David W. Cobb[1,2,#], and Vasant Muralidharan[1,2,*]

[1]Department of Cellular Biology, [2]Center for Tropical and Emerging Global Diseases, University of Georgia, Athens, GA

[#]Current address: Department of Microbiology and Immunology, Vagelos College of Physicians and Surgeons, Columbia University, New York, NY

[*]Corresponding author: vasant@uga.edu

ABSTRACT

The deadly human malaria-causing parasite, *Plasmodium falciparum* relies on its capacity to completely remodel its host red blood cell (RBC) through the export of hundreds of parasite proteins across several membranes to the RBC. Among these exported proteins are numerous membrane proteins that are inserted into the parasite plasma membrane (PPM) during their transport via the secretory pathway. It is not known how these exported membrane proteins are extracted from the PPM for export. To answer this question, we fused the exported membrane protein skeleton binding protein 1 (SBP1) with the rapid, efficient, and promiscuous biotin ligase known as TurboID ($SBP1^{TbID}$). Our data show that the $SBP1^{TbID}$ fusion protein was exported efficiently to the host RBC and was able to rapidly biotinylate proteins at the host-parasite interface during its export as well as at its final destination in the host RBC. Using time-resolved proximity biotinylation and label-free quantitative proteomics, we identified early (pre-export) interactors and late (post-export) interactors of $SBP1^{TbID}$. This led to the identification of 24 proteins that were 10-fold or more enriched in the pre-export time point compared to the post-export time point. Among these early interactors were two promising membrane-associated proteins, one of which has a predicted porin domain, that could potentially act as a translocon at the PPM for exported membrane proteins (Plasmodium translocon of exported membrane proteins or PTEM). Both proteins localize to the host-parasite interface during early stages of the intraerythrocytic cycle and conditional knockdown of these candidates show that they play essential roles in the asexual lifecycle of the parasite. Taken together, our data suggest that these two proteins may play a role in extracting membrane proteins from the PPM for export to the host RBC.

38 # INTRODUCTION

39 Malaria is a major global health issue with an estimated 241 million cases and 627 000
40 deaths reported during 2020[1]. This life-threatening disease is caused by apicomplexan
41 parasites of the genus *Plasmodium*, however one species, *P. falciparum*, is the most
42 virulent and lethal, accounting for 95% of all malaria deaths[2]. The malaria symptoms
43 include headaches, myalgia, high fevers, severe anemia, pulmonary and renal failure,
44 vascular obstruction, and cerebral damage. These disorders are a consequence of
45 parasite proliferation within human red blood cells (RBC) and can persist even after
46 parasite clearance[2,3].

47 To establish infection during their intraerythrocytic cycle, *P. falciparum* parasites must
48 extensively remodel the morphology and physiology of the RBCs. This transformation
49 requires the export of several hundred proteins (about 10% of the parasite proteome)
50 across the parasitophorous vacuole (PV) into the RBC cytoplasm and membrane[4–7],
51 and leads to increased permeability, loss of cell deformability, and formation of
52 virulence-associated knobs at the RBC membrane[8,9]. This multi-step transformation is
53 essential for parasite survival and pathogenesis, conferring *P. falciparum* its ability to
54 maintain chronic infections in humans. A large fraction of exported proteins are
55 recognizable by the presence of a 5-amino acid motif, known as the *Plasmodium* export
56 element or PEXEL[10,11], while others have no discernable primary sequence motif and
57 are termed as PEXEL-negative exported proteins or PNEPs[12]. Most PNEPs possess a
58 transmembrane (TM) domain that serves to target them to the ER and the secretory
59 pathway[12]. Several of these PNEPs play a critical role in malaria pathogenesis, such as
60 skeleton-binding protein 1 (SBP1)[13–15], membrane associated histidine-rich protein
61 (MAHRP1)[16,17] and erythrocyte membrane protein 1 (PfEMP1)[18–20].

62 Exported membrane proteins are inserted into ER membrane during their
63 synthesis[12,21,22]. These membrane proteins are transported via vesicles from the ER
64 and inserted into the parasite plasma membrane (PPM) when the transport vesicles
65 fuse to the PPM[22]. While it has been shown that all exported proteins require the
66 *Plasmodium* translocon of exported proteins (PTEX) to cross the PV membrane

67 (PVM)[23,24], how membrane proteins are extracted from the PPM and delivered to the
68 PTEX complex remains unknown. It has been postulated that a putative *Plasmodium*
69 translocon of exported membrane proteins (which we term as PTEM)[25,26] is required for
70 extraction of membrane proteins from the PPM either alone or in cooperation with the
71 PTEX unfoldase HSP101[27,28] (Fig. 1A). The identity of proteins in this putative PTEM
72 complex are unknown and there are no obvious candidates in the genome of *P.*
73 *falciparum*. Therefore, we attempted to develop an unbiased proteomic approach to
74 identify proteins that could form a putative PTEM complex.

75 Proteomic approaches have been used previously to identify the exported-protein
76 interacting complex (EPIC) at the PV, which is thought to be required for protein
77 export[29]. Similar approaches using *Plasmodium* exported proteins have identified stable
78 complexes at the Maurer's clefts (MC), a parasite-generated protein sorting organelle in
79 the RBC[30,31,32,33]. However, the identification of the putative PTEM has proven elusive
80 because its interaction with exported membrane proteins will be transient and therefore,
81 unlikely to be captured using immunoprecipitation assays which are heavily biased
82 towards stable complexes. Therefore, we used a rapid, proximity-labeling approach to
83 attempt to identify a putative PTEM complex. To our knowledge, this approach has not
84 yet been used in a time-resolved manner to capture transient interactions in the
85 secretory pathway.

86 We chose to tag the endogenous SBP1 gene (PF3D7_0501300) with a new iteration of
87 the promiscuous biotin ligase BirA, known as TurboID (generating $SBP1^{TbID}$)[34]. SBP1 is
88 a PNEP with a single transmembrane domain and is exported in early ring-stage
89 parasites to the MC[13]. TurboID is a highly efficient enzyme that biotinylates proteins in
90 proximity within 10 minutes[34]. Therefore, we hypothesized that $SBP1^{TbID}$ will biotinylate
91 proteins, even those transiently interacting with $SBP1^{TbID}$ along the secretory pathway
92 during its export to the MC. Since $SBP1^{TbID}$ should rapidly biotinylate proximal proteins,
93 we further reasoned that we could differentiate early (pre-export) interactors from late
94 (post-export) interactors of $SBP1^{TbID}$. Our data show that the $SBP1^{TbID}$ fusion protein is
95 exported to the MC efficiently and with similar kinetics to another MC protein, MAHRP1.
96 Critically, $SBP1^{TbID}$ can rapidly biotinylate proximal proteins prior to its export from the

97 PV as well as after export at the MC. Using label-free quantitative proteomics, we
98 compared pre-export interactors and post-export interactors of SBP1^{TbID}. This approach
99 led to the identification of two membrane associated proteins that may be part of the
100 putative PTEM complex.

101 RESULTS

102 SBP1 fused to TurboID is exported to Maurer's Clefts

103 Using CRISPR/Cas9 gene editing we generated mutants of SBP1 (Fig. 1B), where the
104 endogenous gene was tagged with the TurboID biotin ligase (SBP1^{TbID})[34,35]. We chose
105 TurboID because it is an optimized version of the biotin ligase BirA[34]. TurboID is a
106 highly active mutant of BirA with an increased biotinylation radius and faster
107 biotinylation kinetics[34,35]. PCR analysis of genomic DNA isolated from the SBP1^{TbID}
108 parasite line showed the correct integration of the TurboID biotin ligase and a V5 tag at
109 the endogenous locus of SBP1 (Fig. 1C). We detected expression of the SBP1^{TbID} in the
110 mutant line at the expected size, but not in the parental line (Fig. 1D). To ensure that the
111 expression of TurboID is not detrimental to the parasite, we observed the growth of
112 SBP1^{TbID} and the parental parasite line (NF54^{attB})[36], over several asexual cycles using
113 flow cytometry (Fig. 1E). These data show no difference in the asexual growth of
114 SBP1^{TbID} compared to the parental parasites, demonstrating that expression of TurboID
115 or its fusion to SBP1 does not inhibit parasite growth.

116 SBP1 is an exported protein with a single transmembrane domain synthesized in the
117 parasite ER and transported to the MC in the RBC cytoplasm[37,38]. To confirm that fusing
118 TurboID to SBP1 did not inhibit its export to the MC, we used immunofluorescence
119 microscopy (IFA) to test whether SBP1^{TbID} colocalized with another MC resident protein,
120 MAHRP1[17]. Our data show that SBP1^{TbID} is exported from the parasite to the MC and
121 co-localizes with MAHRP1 during trophozoite and schizont stage parasites (Fig. 1F and
122 1G). On the other hand, in early ring stage parasites, we show that SBP1^{TbID}, as well as
123 MAHRP1, localize to the periphery of the parasite, probably in the PV prior to export
124 (Fig. 1F). SBP1 accumulation in electron dense regions within the parasite plasma
125 membrane (PPM) before transport through the PV membrane has previously been

126 observed by electron microscopy [39]. These data suggest that SBP1 and possibly other
127 MC resident proteins accumulate in the PV before being exported to the infected RBC.
128 Together, our data show that tagging SBP1 with the TbID biotin ligase did not alter the
129 asexual growth or development of the parasite, nor did it inhibit the export of SBP1 to
130 the host RBC and MC (Fig. 1).

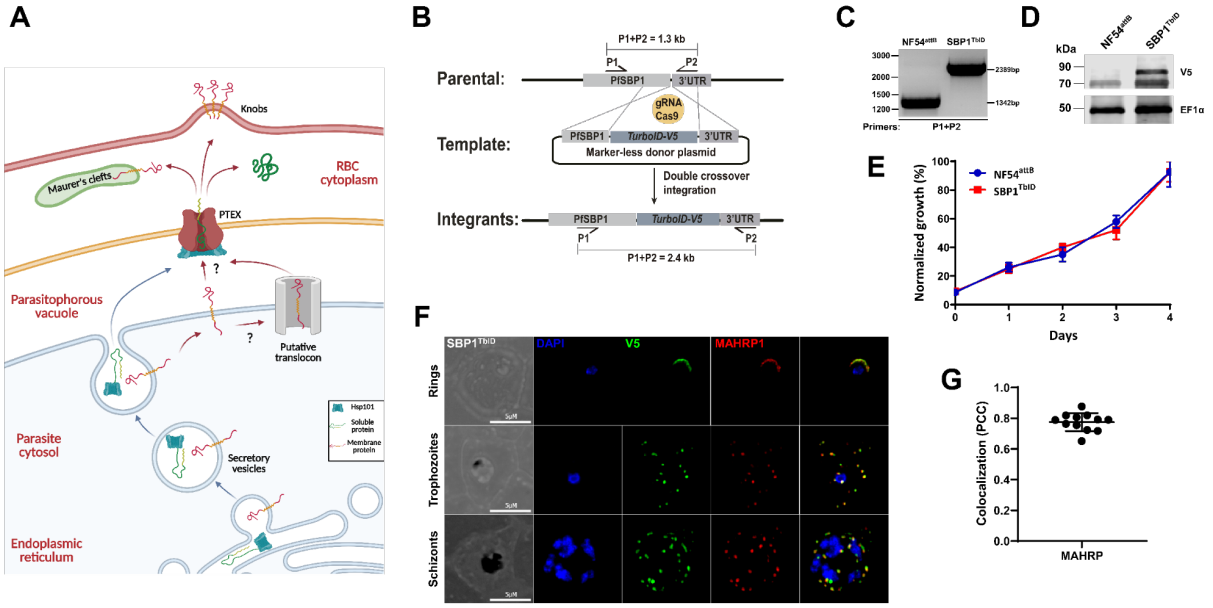

131

132 **Figure 1. Generation of SBP1^{TbID} mutants.** (A) Schematic of protein export. Membrane and
133 soluble proteins are transported from the ER into the PV by secretory vesicles. Soluble proteins
134 are released into the PV lumen after fusion of the secretory vesicle to the PPM. Membrane
135 proteins, on the other hand, are inserted into the PPM and need to be extracted from the
136 membrane by a putative translocon (PTEM) for further transport through the PV membrane to
137 the RBC cytoplasm by the PTEX complex. Soluble and membrane proteins are transported to
138 their final location in the infected RBC. (B) Schematic showing the integration of the repair
139 plasmid used to tag the genomic loci of SBP1 with TurboID-V5. Cas9 introduces a double-
140 stranded break at the C-terminus of the SBP1 locus. The repair plasmid provides homology
141 regions for double-crossover homologous recombination, introducing TurboID and the V5 tag
142 sequences. (C) PCR test confirming integration at the SBP1 locus. Amplicons were amplified
143 from genomic DNA isolated from mutant and wild-type parasites. Primers were designed to
144 amplify the region between the C-terminus and the 3'UTR of SBP1. All primers are in
145 Supplemental Table 1. (D) Western blot of parasite lysates isolated from the parental line
146 (NF54^{attB})[36] and a clone of SBP1^{TbID} (D10) probed with antibodies against V5 and EF1α (loading
147 control). The protein marker sizes are shown on the left. (E) Growth of asynchronous SBP1^{TbID}
148 parasites, compared to the parental line NF54^{attB}, over 4 days via flow cytometry. 100%
149 represent the highest value of calculated parasitemia. Representative of three biological
150 replicates shown for each growth curve. Each data point represents the mean of three technical

151 replicates; error bars represent standard deviation. (F) IFA showing SBP1^{TbID} localizes to the
152 parasite periphery in early-ring stage (top) and is exported to the Maurer's cleft in trophozoite
153 (middle) and schizont (bottom) stages. Asynchronous SBP1^{TbID} parasites were fixed with
154 acetone and stained with specific antibodies. Images from left to right are phase-contrast, DAPI
155 (nucleus, blue), anti-V5 (green), anti-MAHRP (red), and fluorescence merge. Z stack images
156 were deconvolved and projected as a combined single image. (G) Quantification of the
157 colocalization of SBP1^{TbID} with MAHRP using the Pearson's correlation coefficient. Three
158 biological replicates represented with 4 late-stage-parasite images from each replicate. Error
159 bars represent standard deviation.

160

161 Biotin-dependent proximity labeling by SBP1^{TbID}

162 Since our data show that the SBP1^{TbID} fusion protein was exported to MC, we wanted to
163 examine the capacity of TurboID to biotinylate proximal proteins in SBP1^{TbID} parasites.
164 TurboID is an extremely efficient enzyme and we observed it could utilize the minimal
165 amount of biotin present in the media used to grow SBP1^{TbID} parasites (Fig. S1). The
166 ability of SBP1^{TbID} to use the biotin present in complete media meant that biotinylation of
167 proximal proteins would occur constantly, which would prevent the differentiation of
168 early interactors from late interactors. Thus, we grew SBP1^{TbID} in minimal media without
169 biotin because the normal asexual development of *P. falciparum* does not require
170 biotin[40]. To test if SBP1^{TbID} biotinylation is dependent upon the presence of exogenous
171 biotin, we analyzed protein extracts of asynchronous parasites in the presence or
172 absence of biotin by streptavidin blotting. We observed that efficient biotinylation of
173 proximal proteins occurs only in the presence of biotin in SBP1^{TbID} parasites (Fig. 2A).
174 Self-biotinylation in SBP1^{TbID} parasites was observed in the presence or absence of
175 biotin (Fig. 2A, lane 3 and 4, see asterisk), in agreement with previously reported when
176 tagging proteins with TurboID[34,41]. No endogenous biotinylation was detected in the
177 parental line NF54^{attB}, showing that biotinylation occurs only when TurboID is being
178 expressed by the parasite line (Fig. 2A, lane 1 and 2). These data show that SBP1^{TbID}
179 efficiently biotinylates proteins and its activity is dependent upon the presence of biotin
180 in the growth medium.

181 TurboID is a highly active enzyme[34] that offers the possibility of rapid and time-resolved
182 labeling approaches in contrast to previous proximity-labeling methods with much

183 longer incubation times, usually greater than 12 hours[42–44]. Thus, we wanted to assess
184 whether SBP1^{TbID} is able to rapidly biotinylate proximal proteins. SBP1^{TbID} parasites
185 were incubated with biotin for 1, 2 or 6 hours and the biotinylation of proteins were
186 observed using western blots probed with streptavidin (Fig. 2B). We also tested
187 biotinylation in response to different concentrations of biotin, 25, 50 and 100 μM (Fig.
188 2C). Biotinylated proteins were observed at all time points and biotin concentration, and
189 the observable difference in the extent of protein biotinylation between the time points
190 and concentrations was minimal (Fig. 2B and 2C).

191 The SBP1^{TbID} fusion protein has to traverse several membranes during its export to the
192 MC, and therefore, it is likely to unfold and then refold during this transport process.
193 Furthermore, to our knowledge TurboID has not yet been utilized in a time-resolved
194 manner to identify transient interactors as proteins are transported through the secretory
195 pathway. Therefore, we wanted to determine if SBP1^{TbID} parasites could biotinylate
196 proteins proximal to SBP1 at different cellular locations during the export of SBP1^{TbID}
197 from the parasite ER to the MC. Synchronized early ring and trophozoite stage
198 parasites were observed by IFAs after the addition of biotin for 2 h. We observed
199 biotinylation at the parasite periphery, possibly when SBP1^{TbID} accumulates at the PV[39]
200 (Fig. 2D, top panels). Biotinylation was also observed when SBP1^{TbID} had been
201 exported to the MC (Fig. 2D, bottom panels). The observed biotinylation was dependent
202 upon the addition of biotin. Together, these data demonstrate that SBP1^{TbID} was highly
203 active, efficient, rapid, and labeled proximal proteins at different subcellular locations
204 during its export from the parasite ER to the final location at the MC.

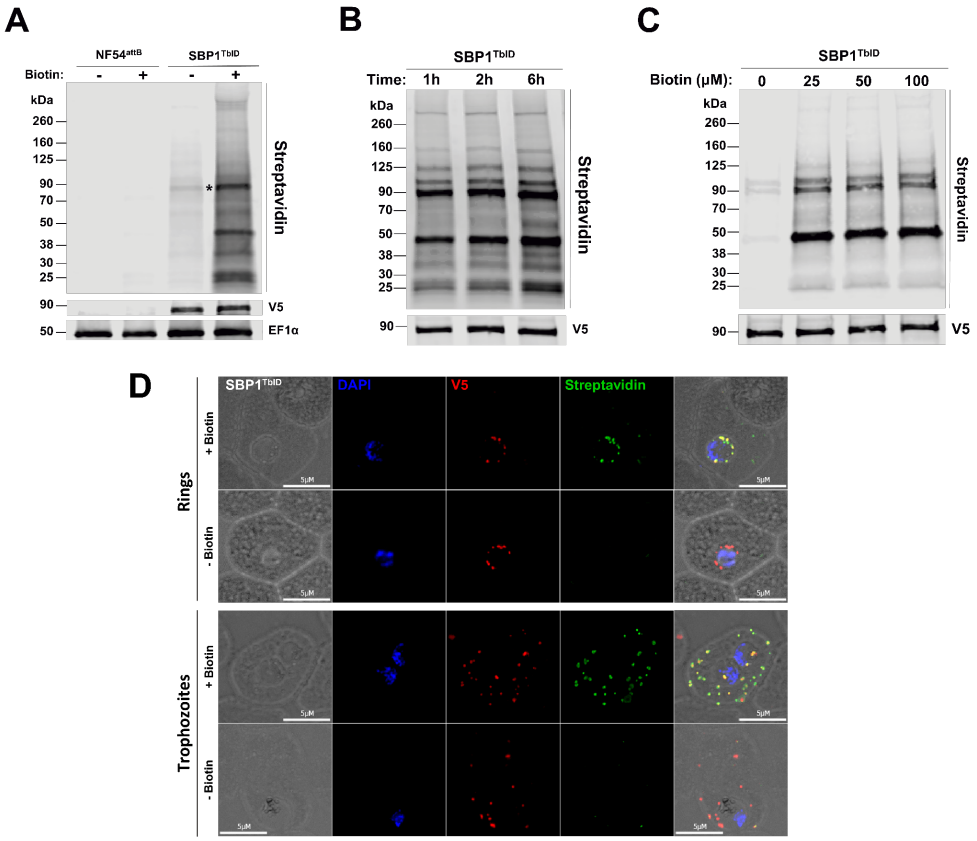

Figure 2. Biotinylation of proximal proteins by TurboID$_{V5}$-tagged SBP1. (A) Western blot of parasite lysates isolated from the parental line NF54^{attB} and the mutant line SBP1^{TbID} incubated with or without biotin (50 μM) for 2 h. Samples were probed with antibodies against V5, EF1α (loading control) and fluorescent dye-labeled streptavidin. The protein marker sizes are shown on the left. (B) Western blot of parasite lysates isolated from the mutant line SBP1^{TbID} incubated with biotin (50 μM) for 1 h, 2h and 6h. Samples were probed with antibodies against V5 (loading control) and fluorescent dye-labeled streptavidin. The protein marker sizes are shown on the left. (C) Western blot of parasite lysates isolated from the mutant line SBP1^{TbID} incubated with different concentrations of biotin (0, 25, 50 and 100 μM) for 1 h. Samples were probed with antibodies against V5 (loading control) and fluorescent dye-labeled streptavidin. The protein marker sizes are shown on the left. (D) IFA showing SBP1^{TbID} biotinylates proteins during their export out of the parasite (top panels) and at their final location at the Maurer's clefts (Bottom panels). Asynchronous SBP1^{TbID} parasites were fixed with acetone after 2 h of incubation with biotin (50 μM) and stained with specific antibodies. Images from left to right are phase-contrast, DAPI (nucleus, blue), anti-V5 (red), streptavidin (green), and fluorescence merge. Z stack images were deconvolved and projected as a combined single image.

223 ## Early interactors of SBP1^{TbID} identified by proximity labeling

224 Since our data show that SBP1^{TbID} biotinylates proximal proteins during its transport
225 from the parasite ER into the RBC cytoplasm (Fig. 2C), we next wanted to identify the
226 *P. falciparum* effectors that interact with SBP1 at the host-parasite interface. To do so,
227 we wanted to define the kinetics of SBP1^{TbID} transport from its site of synthesis in the
228 parasite ER to the MC and test if we could reproducibly detect SBP1 at the host-
229 parasite interface. As previously described (Fig. 1E, 2D), SBP1^{TbID} and proteins
230 biotinylated by SBP1^{TbID} could be detected at the parasite-RBC interface. To assess
231 whether we could reproducibly observe SBP1^{TbID} within the parasite prior to its export to
232 the host RBC, we observed the subcellular localization of SBP1^{TbID} with respect to
233 EXP2, a PVM resident protein[46,47], at different time points after parasite invasion in
234 tightly synchronized cultures. SBP1 has been detected at the MCs as early as 4-6 hours
235 post invasion (hpi)[48], therefore, we observed the subcellular location of SBP1^{TbID} in
236 parasites at 3, 4 and 5 hpi. In some SBP1^{TbID} parasites, SBP1 was either not detectable
237 or not expressed (Fig. 3B, top panels). As expected, we found parasites where
238 SBP1^{TbID} was within the PV periphery, and others where the protein was already
239 exported to the RBC cytoplasm (Fig. 3C, mid and bottom panels). We quantified these
240 three events over several biological replicates. At 4hpi, SBP1^{TbID} was not expressed in
241 about 30% of the parasites, exported in ~10% of observed parasites and at the host-
242 parasite interface in the vast majority (60%) of all parasites (Fig. 3C). These data
243 showed us that harvesting proteins biotinylated by SBP1^{TbID} at the host-parasite
244 interface would be feasible.

245 To identify early interactors of SBP1, especially those at the host-parasite interface, we
246 opted for a quantitative and comparative approach. We wanted to differentiate these
247 early interactors from SBP1 interactors at the MC, which have been previously
248 identified[32], as well as those being co-transported with SBP1 to the MC. We
249 hypothesized that using label-free quantitative proteomics and comparing interactors
250 isolated from 4 hpi and 20 hpi would allow us to identify the early interactors of SBP1.
251 By 20 hpi, all SBP1 is at the MCs and no more SBP1 is synthesized[49]. Label-free
252 proteomics have been shown to offer a large dynamic range and high proteome

253 coverage in the identification of biotinylated proteins[41,50–52].

254 First, tightly synchronized late-stage schizonts were collected. These parasites were
255 then split into two samples, one incubated with biotin for 4 h until 4 hpi (Fig. 3A, blue
256 square) and then collected for further processing. Since our data show that in the
257 majority of the 4 h ring stage parasites, SBP1^{TbID} was at the host-parasite interface (Fig.
258 3C), parasites were incubated with biotin for 4 h to maximize the labeling of proximal
259 proteins and capture a larger fraction of the pre-export interactors. To collect the post-
260 export sample, we let SBP1^{TbID} parasites develop until 16hpi because all SBP1 localizes
261 to MC by this time and this protein is no longer synthesized. Thus, this sample was
262 allowed to develop without biotin for 16h, and then incubated with biotin for 4 h until 20
263 hpi (Fig. 3A, red square). Biotinylated proteins were isolated from parasite lysates using
264 streptavidin-affinity pulldown. Streptavidin-captured proteins were identified via mass
265 spectrometry (MS) and quantified over several biological replicates[41,50,51] (Fig. 4A). A
266 total of 1,122 proteins were identified in at least one of the replicates. We then
267 compared the proteins identified in the 4h sample with those identified in the 20h
268 sample (Fig. 4B). We defined the putative pre-export interactors of SBP1 from our
269 dataset using three stringent criteria. Proteins enriched more than 10-fold compared to
270 the 20 hpi samples with a p-value cut-off of 0.05, and present in all three biological
271 replicates were considered as differentially labeled interactors at 4 hpi. Using these
272 criteria, 24 protein candidates were identified as putative pre-export interactors of
273 SBP1^{TbID} during its transport at the parasite-RBC interface (Fig. 4B). The identified
274 proteins were classified into subgroups based on their predicted functions and
275 subcellular locations[53]. Of the 24 identified proteins, 11 were uncharacterized proteins
276 with no predicted function. As expected, this approach identified proteins known to be
277 involved in protein and vesicle transport (5/24). One of the statistically significant
278 interactors of SBP1 was EXP3 (3-fold enriched at 4hpi), which has been localized to the
279 PV and functions in protein export [29]. SBP1 (star, Fig. 4B) and other MC localized
280 proteins were also identified but were not enriched at either time point, demonstrating
281 that the experiment worked as designed (Fig. 4B). Identification of other exported
282 proteins, including some MC proteins, only in the post-export (20hpi) samples further

283 suggests that the proteomic approach using SBP1^{TbID} worked as designed. Together
284 these data show that our approach successfully identified a group of proteins
285 differentially biotinylated by SBP1^{TbID} prior to its export to the MC.

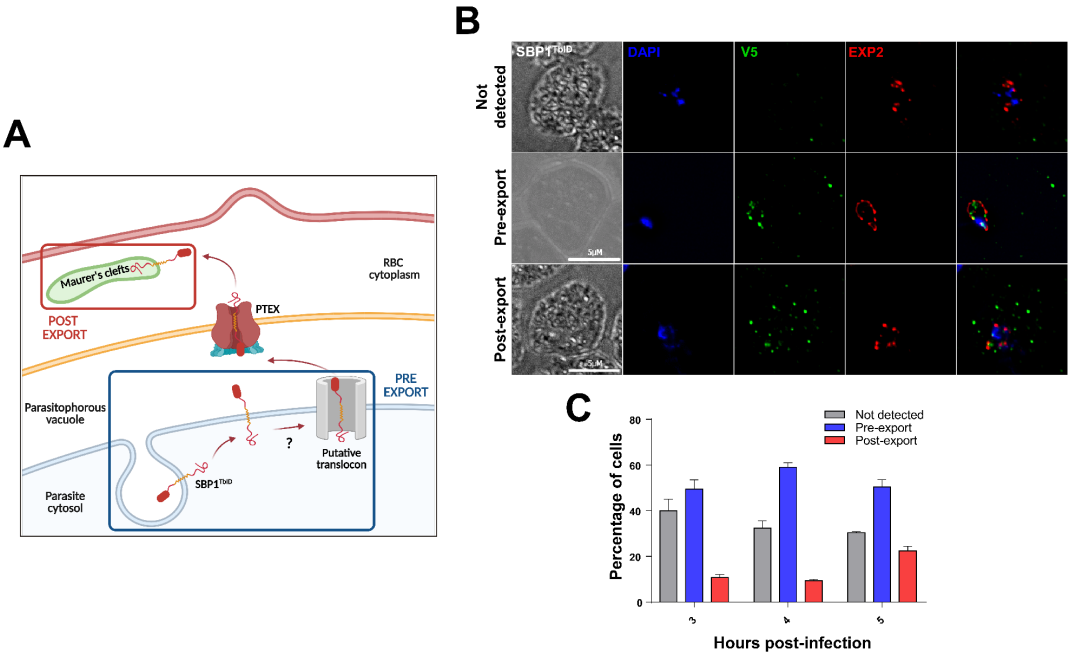

286

287 **Figure 3.** (A) Schematic of the export of proteins in *P. falciparum* highligting the locations where
288 proteins biotinylated by SBP1^{TbID} will be harvested. Created with BioRender.com. (B) IFA
289 showing the different localizations of SBP1^{TbID} during its export at early ring-stages (3-5 hpi).
290 Tightly synchronous SBP1^{TbID} parasites were fixed with acetone at 3 h, 4h and 5 h post
291 infection, and stained with specific antibodies. Images from left to right are phase-contrast, DAPI
292 (nucleus, blue), anti-V5 (green), EXP2 (PV marker, green), and fluorescence merge. Z stack
293 images were deconvolved and projected as a combined single image. (C) Quantification of the
294 events observed in (B). Events were scored based on the localization of SBP1^{TbID} with respect
295 to the PV marker EXP2. A total of 50 parasites were scored for each time point. n= 3 biological
296 replicates; error bars represent standard deviation.

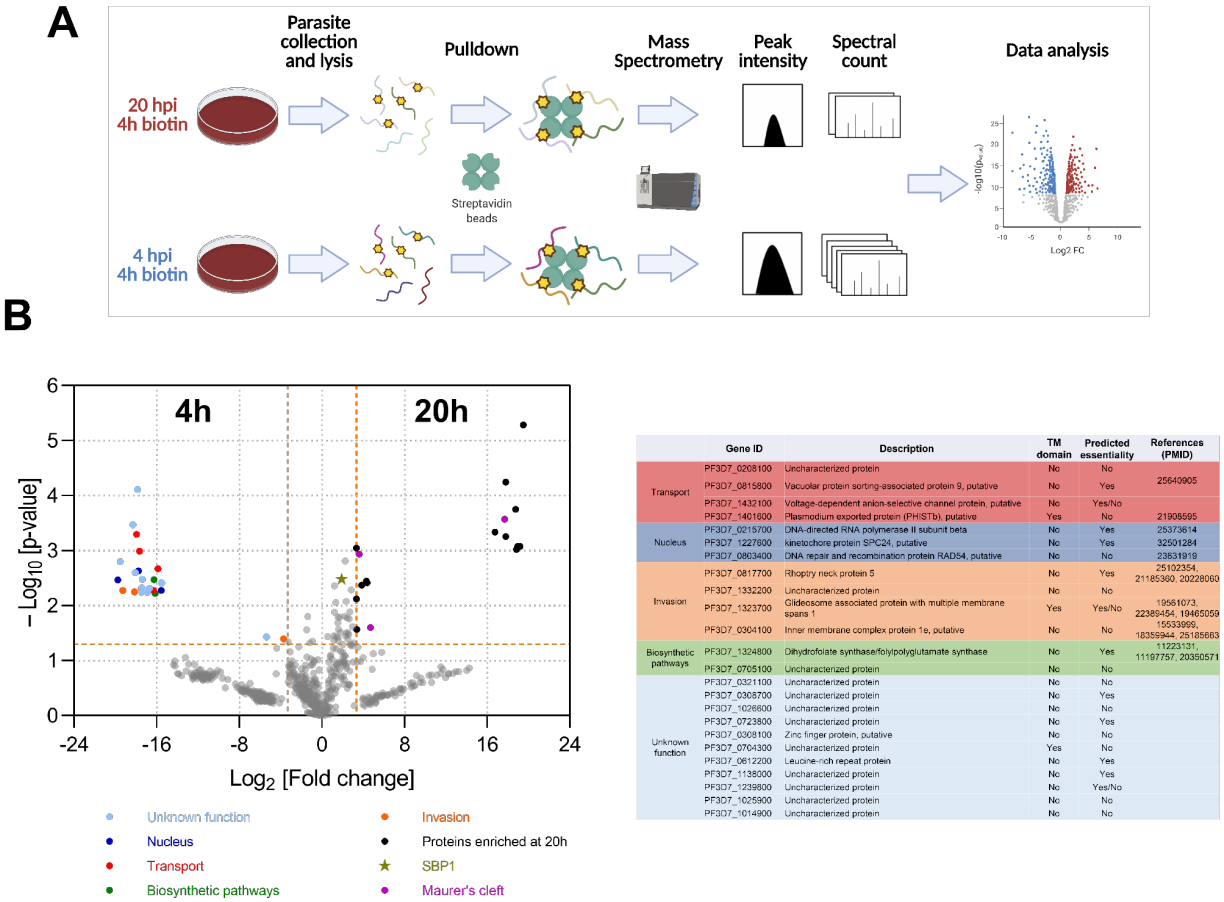

	Gene ID	Description	TM domain	Predicted essentiality	References (PMID)
Transport	PF3D7_0208100	Uncharacterized protein	No	No	25640905
	PF3D7_0815800	Vacuolar protein sorting-associated protein 9, putative	No	Yes	
	PF3D7_1432100	Voltage-dependent anion-selective channel protein, putative	No	Yes/No	
	PF3D7_1401600	Plasmodium exported protein (PHISTb), putative	Yes	No	21906595
Nucleus	PF3D7_0215700	DNA-directed RNA polymerase II subunit beta	No	Yes	25373614
	PF3D7_1227600	kinetochore protein SPC24, putative	No	Yes	32501284
	PF3D7_0803400	DNA repair and recombination protein RAD54, putative	No	No	23631918
Invasion	PF3D7_0817700	Rhoptry neck protein 5	No	Yes	25102354, 21185360, 20228060
	PF3D7_1332200	Uncharacterized protein	No	No	
	PF3D7_1323700	Gliideosome associated protein with multiple membrane spans 1	Yes	Yes/No	19561073, 22389454, 19465059
	PF3D7_0304100	Inner membrane complex protein 1e, putative	No	No	15533999, 18359944, 25185683
Biosynthetic pathways	PF3D7_1324800	Dihydrofolate synthase/folylpolyglutamate synthase	No	Yes	11223131, 11197757, 20350571
	PF3D7_0705100	Uncharacterized protein	No	No	
Unknown function	PF3D7_0321100	Uncharacterized protein	No	No	
	PF3D7_0308700	Uncharacterized protein	No	Yes	
	PF3D7_1026600	Uncharacterized protein	No	No	
	PF3D7_0723800	Uncharacterized protein	No	Yes	
	PF3D7_0308100	Zinc finger protein, putative	No	No	
	PF3D7_0704300	Uncharacterized protein	Yes	No	
	PF3D7_0612200	Leucine-rich repeat protein	No	Yes	
	PF3D7_1138000	Uncharacterized protein	No	Yes	
	PF3D7_1239800	Uncharacterized protein	No	Yes/No	
	PF3D7_1025900	Uncharacterized protein	No	No	
	PF3D7_1014900	Uncharacterized protein	No	No	

Figure 4. (A) Schematic of the experimental design for time-resolved biotinylation and proteomics to identify pre-export and post-export interactors of SBP1^{TbID}**.** Created with BioRender.com. (B) Interactors enriched at 4 hpi (p-value plotted as function of fold change between the two samples). Proteins with p-value ≤0.05 and more than 10-fold change are identified as SBP1^{TbID} interactors. n= 3 biological replicates. (C) A summary table of the putative interactors of SBP1^{TbID} at 4hpi grouped by their putative functions are shown. All proteins identified are in Supplemental Table 2.

Early interactors of SBP1^{TbID} localize to the host-parasite interface

Since we were interested in identifying proteins that may act as a putative translocon to extract exported membrane proteins at the PPM, we reasoned that membrane associated proteins among pre-export SBP1 interactors could function in this role. Thus, based on membrane-association, high statistical score and fold enrichment, we selected

311 the Glideosome-associated protein with multiple membrane spans 1 (GAPM1,
312 PF3D7_1323700) as one putative candidate. GAPM1 is a membrane protein associated
313 with the biogenesis of the Inner Membrane Complex (IMC) in asexual and sexual
314 stages. GAPM1, as part of the IMC, is suggested to have a role in merozoite invasion[54–
315 56]. Using these criteria, another putative candidate was the channel protein Voltage-
316 dependent anion-selective channel protein (VAC, PF3D7_1432100). VAC is a soluble
317 protein with a translocon of outer mitochondrial membrane (TOM40) domain but no
318 mitochondria targeting signal. Nothing is known about the function of VAC in *P.*
319 *falciparum*.

320 To characterize these proteins, we used CRISPR/Cas9 gene editing to generate the
321 conditional mutants, termed VAC^{apt} and GAPM1$^{mNG\text{-}apt}$. In these parasite lines, their
322 endogenous loci were tagged with the *tetR* aptamer system, which results in
323 anhydrotetracycline (aTc)-dependent expression of protein (Fig. 5A and 5B)[57]. PCR
324 analysis of genomic DNA from VAC^{apt} and GAPM1$^{mNG\text{-}apt}$ parasite lines showed correct
325 integration of the knockdown system at the endogenous loci (Fig. S2A-C). To assess
326 the efficiency of the knockdown system, we measured protein expression in the
327 presence or absence of aTc by Western blotting. For both proteins, there is a clear
328 reduction of protein expression (Fig. S2D). Knockdown of GAPM1 was detrimental, as
329 parasites were not able to progress into a second life cycle (Fig. S2E). Knockdown of
330 VAC also inhibited the asexual expansion of VAC^{apt} parasites (Fig. S2E).

331 Our data show that GAPM1^{mNG} localizes to the IMC in schizonts (Fig. S3). However,
332 what happens to the IMC after merozoite invasion is unclear and we reasoned that the
333 IMC most likely fuses to the PPM shortly after invasion. Similarly, the subcellular
334 localization of VAC during the early stages of the asexual lifecycle was unknown. The
335 proteomic data suggest that these proteins are proximal to SBP1^{TbID} when SBP1 is in
336 the PV (Fig. 4B). Therefore, we used IFAs to localize both proteins in tightly
337 synchronized parasites at 4 hpi with respect to the PV marker EXP2. VAC^{apt} localizes to
338 the parasite periphery and is closely juxtaposed with the known PV marker, EXP2, but it
339 also partially overlaps with the mitochondria (Fig. 5A, top panels) suggesting that it may
340 be localized to both subcellular organelles. GAPM1$^{mNG\text{-}apt}$ localizes to the parasite

341 periphery at 4 hpi, and shows colocalization with EXP2 (Fig. 5A, bottom panels). To
342 corroborate our observations by IFAs, we used structured illumination microscopy (SIM)
343 to determine the subcellular localization of VAC and GAPM1. Both proteins are closely
344 juxtaposed to the PVM marker EXP2, which suggests VAC and GAPM1 do not localize
345 to the PVM (Fig. 5B). The SIM data show that both VAC and GAPM1 follow the same
346 contours as EXP2 but the signals do not completely overlap, which suggests that VAC
347 and GAPM1 localize to another membrane (Fig. 5B and Fig. S4). Together these results
348 show that both GAPM1 and VAC localize to the same region together with SBP1^{TbID} at
349 the PV at 4 hpi, as suggested by the proximity labeling data.

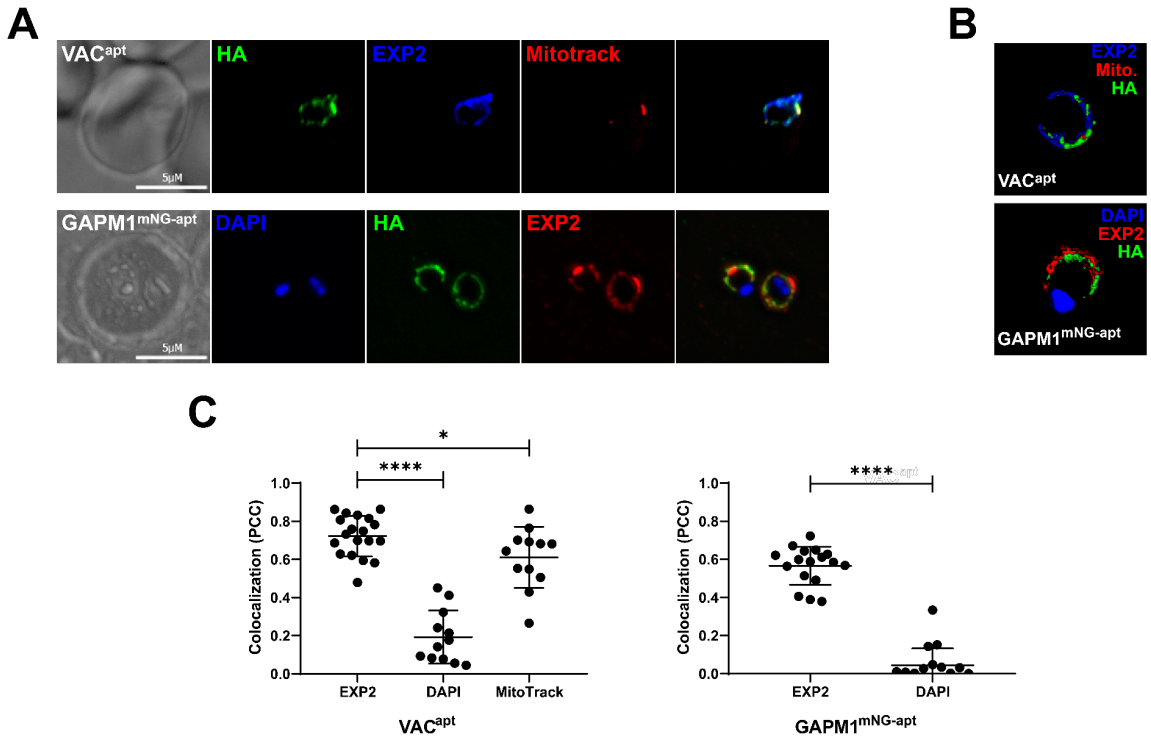

350

351 **Figure 5. Generation and characterization of VAC^{apt} and GAPM1$^{mNG-apt}$.** (A) Representative
352 IFA showing VAC^{apt} and GAPM1$^{mNG-apt}$ localizes within the PV in the early-ring stage (4 hpi).
353 Tightly synchronous parasites were fixed with PFA (VAC^{apt}) and acetone (GAPM1$^{mNG-apt}$) and
354 stained with specific antibodies. Images of VAC^{apt} from left to right are phase-contrast, anti-HA
355 (green), anti-EXP2 (PV, blue), mitotracker (mitochondria, red), and fluorescence merge. Images
356 of GAPM1$^{mNG-apt}$ from left to right are phase-contrast, DAPI (nucleus, blue), anti-HA (green),
357 anti-EXP2 (PV, red), and fluorescence merge. Z stack images were deconvolved and projected
358 as a combined single image. (B) 3D reconstruction based on structured illumination microscopy
359 images captured from VAC^{apt} and GAPM1$^{mNG-apt}$ ring-stage parasites at 4 hpi and stained with
360 the antibodies as in (A). (C) Quantification of the colocalization of VAC and GAPM1^{mNG} with

361 respect to EXP2, MitoTracker (Mitochondrial marker) and DAPI, and to EXP2 and DAPI,
362 respectively, using the Pearson's correlation coefficient. Three biological replicates represented
363 with 6 parasite images from each replicate for EXP2, and 3 parasite images for MitoTrack and
364 DAPI. Error bars represent standard deviation. ****$p<0.05$ by t-student test.

365

366 DISCUSSION

367

368 The protein-protein interactions that usher exported proteins to their final destinations in
369 the RBC via the secretory pathway are transient in nature. Previously, IP-based methods
370 have been used to identify proteins required for export of *P. falciparum* proteins, such as
371 the PTEX complex[58] and the EPIC complex[29]. While IP-based approaches are well-suited
372 for identifying stable complexes, they are unlikely to identify transient interactions.
373 Consequently, a putative additional translocon at the PPM required for extracting
374 exported membrane proteins which are inserted into the PPM during transport has long
375 been proposed[25,26], but no candidates for this putative PTEM complex have been
376 identified as yet (Fig. 1).

377

378 To identify candidates for a putative PTEM complex, we used time-resolved biotinylation
379 to identify transient interactions of an exported membrane protein, SBP1, during its export.
380 This approach uses a rapid and promiscuous biotin ligase to biotinylate proximal
381 proteins[34]. Since biotinylation is a permanent modification, even transient interactions can
382 be potentially identified. Our data show that fusion of TurboID to the exported
383 transmembrane-containing protein, SBP1, did not alter its trafficking to the MC nor did it
384 have any effect on parasite growth. These data also suggest that TurboID is enzymatically
385 active during transit in the parasite secretory pathway.

386 A previous study on the SBP1 interactome at their final location at the Maurer's cleft
387 identified 88 parasite proteins as putative interactors[32]. Most of the top-ranked hits from
388 the previous study were also identified in our study, including PfEMP1, Pf332, PIESP2,
389 REX1, MAHRP1, PTP1 and vapA, but were not highly enriched (≤10-fold) in the post-

390 export interactors fraction. It is possible that some of these proteins are co-transported
391 with SBP1 and thus, are identified in the pre-export fraction as well. Members of the PTEX
392 complex such as EXP2, HSP101, and Trx2, were also identified in the pre-export fraction,
393 albeit below statistical significance. In addition, PTP2 and PfG174, which have previously
394 been shown to localize as residents[59], or transient interactors[60] of the Maurer's clefts,
395 were more than 10-fold enriched at the post-export time point, demonstrating the reliability
396 of our approach to identify SBP1 interactors. Another subset of proteins identified in our
397 study as post export interactors of SBP1 are ribosomal proteins, which have been
398 previously observed to be exported to the red blood cell cytoplasm in *P. falciparum*[61].
399 Together, these data strongly suggest that the time-resolved, rapid biotinylation approach
400 was working as designed. Since our focus was to identify pre-export interactors, we did
401 not pursue these proteins for further study.

402 Using label-free quantitative proteomics, we identified a group of 24 putative candidates
403 that interact with SBP1 prior to its export to the RBC. Several of the proteins identified
404 (11/24) were uncharacterized proteins. Since we undertook this approach to identify the
405 proposed translocon of exported membrane proteins, we did not pursue the function of
406 these proteins in this study. Translocons function to transport proteins across membranes
407 and therefore, we hypothesized that membrane associated proteins in this list could
408 putatively function as translocons. There were two putative candidates in the pre-export
409 interactors of SBP1 that were membrane associated, VAC and GAPM1. However, their
410 localization in early ring stage parasites was unknown. Therefore, to study the function of
411 VAC and GAPM1 in early ring stage parasites, we successfully generated conditional
412 mutants. The data show that both VAC and GAPM1 play important functions in parasite
413 survival within the infected RBC. Knockdown of these proteins inhibits parasite growth.
414 However, achieving protein knockdown takes about 48 hours and results in parasite death
415 prior to re-invasion of the RBC. Therefore, this prevents the characterization of their role
416 in export, which occurs in about 6-8 hours after invasion. Similar to the PTEX translocon,
417 EXP2[46], it is likely that both GAPM1 and VAC have other essential functions in the asexual
418 lifecycle. Defining their function in export will require using a more rapid knockdown

419 approach with similar kinetics as SBP1 export, such as degradation-domain based
420 tools[23,62] or rapid mislocalization based methods[63].
421
422 VAC has a β-barrel porin domain that can form an aqueous channel in the membrane and
423 function as a translocon in mitochondria and other plastids[64]. In a recent proximity-
424 biotinylation based proteomic screen to catalog mitochondrial proteins in *P. falciparum*,
425 VAC was pulled down in the membrane fraction of parasite lysates, and not in the
426 mitochondrial fraction[65]. In addition, VAC does not have a predicted mitochondrial
427 targeting sequence, in contrast to its ortholog, TOM40 (PF3D7_0617000), which has a
428 mitochondrial targeting sequence, suggesting that VAC might not be localized to the
429 mitochondria[66]. Our data reveal that VAC localizes at the host-parasite interface in early
430 ring stages. While there is some overlap of VAC with the mitochondria, there is stronger
431 overlap between the PVM marker, EXP2, and VAC in lower resolution IFAs. It is also
432 possible that VAC is dually localized both to the mitochondria as well as to the host-
433 parasite interface. SIM data suggest that EXP2 and VAC are closely juxtaposed but with
434 minimal overlap. This suggests that VAC localizes to a compartment in close proximity to
435 the PVM, most likely the PPM. On the other hand, GAPM1 has seven TM domains and is
436 from an apicomplexan-specific family of proteins[56]. GAPM1 has been localized to the
437 inner membrane complex (IMC) in schizont-stage parasites[56]. The IMC plays an essential
438 role in the invasion of merozoites into the RBC, however, it is unclear what happens to
439 the IMC post-invasion. Lower resolution IFAs show that GAPM1 co-localizes with the PVM
440 localized EXP2 in early ring stage parasites. Using SIM, we observed GAPM1 in close
441 juxtaposition with EXP2, but they do not completely overlap, suggesting that GAPM1, like
442 VAC, localizes to a membrane compartment at the parasite periphery that is not the PVM.
443 Given these data, it is likely that GAPM1 may also localize to the PPM in early rings.
444 These data further suggest that the IMC may fuse to the parasite plasma membrane after
445 merozoite invasion. Together, these findings suggest that VAC and GAPM1 transiently
446 interact with SBP1 prior to its export and their localization to the parasite periphery
447 suggests a role in export, perhaps as members of a putative PTEM complex. Based on
448 these data, we propose a model where GAPM1 and VAC act together to select and extract

449 exported membrane proteins from the PPM for further transport via the PTEX into the
450 host RBC.
451
452 Several mechanistic aspects of this model remain to be resolved but like the PTEX
453 complex, which was first identified as a putative complex at the PV membrane[58]. Both
454 VAC and GAPM1 were reproducibly biotinylated by SBP1^{TbID} prior to its export and
455 localize to the parasite periphery. Further, VAC has a porin translocon domain which could
456 function in a manner analogous to the mitochondrial outer membrane translocon to extract
457 membrane anchored exported proteins from the parasite plasma membrane. This hints
458 that this porin domain protein has been repurposed by *Plasmodium* parasites on the PPM
459 to facilitate export of membrane proteins to the infected RBC.

460

461 ## ACKNOWLEDGEMENTS

462 We thank Chi-Min Ho for helpful comments on the manuscript; Dan Goldberg for anti-
463 EF1α; Hans-Peter Beck for anti-MAHRP1; the European Malaria Reagent Repository
464 for anti-EXP2; Julie Nelson at the CTEGD Cytometry Shared Resource Laboratory for
465 help with flow cytometry and analysis; and Muthugapatti Kandasamy at the Biomedical
466 Microscopy Core at the University of Georgia for help with microscopy. We
467 acknowledge the assistance of Phil Gafken at the Proteomics Resource at Fred
468 Hutchinson Cancer Research Center for mass spectrometry analysis. The study was
469 funded by NIH/NIAID R01AI130139 (V.M.), T32AI060546 (D.W.C.), and CTEGD
470 Fellowship funded by Provost's Office at UGA (D.A.).

471

472

473 # MATERIALS AND METHODS

474 ## Construction of SBP1 plasmids

475 Genomic DNA was isolated from *P. falciparum* NF54^{attB} cultures using the QIAamp DNA
476 blood kit (Qiagen). PCR products were inserted into the respective plasmids using
477 ligation-independent cloning (SLIC), as described earlier [67], or the NEBuilder HiFi DNA
478 Assembly system (NEB). All constructs used in this study were confirmed by
479 sequencing. All primers used in this study are in Supplemental Table 1.

480 For generation of the plasmid pTOPO-SBP1-TbID, sequences of approximately 500 bp
481 of homology to the SBP1 C-terminus and 3'UTR were amplified using primer pairs P1-
482 P2 and P3-P4, respectively, and the sequence of V5-tagged TurboID was amplified
483 using primers P5 and P6. For expression of a SBP1 gRNA, oligos P17-P18 were
484 inserted into cut pUF1-Cas9.

485 For generation of the plasmid pKD-VAC-Apt, sequences of approximately 450 bp of
486 homology to the Pf1432100 C-terminus and 3'UTR were amplified using primer pairs
487 P7-P8 and P9-P10, respectively. Amplicons were then inserted into pKD[57,67] digested
488 with AatII and AscI. For expression of a Pf1432100 gRNA, oligo P19 was inserted into
489 cut PUF1-Cas9.

490 For generation of the plasmid pKD-GAPM1-mNG-Apt, sequences of approximately 500
491 bp of homology to the PfGAPM1 C-terminus and 3'UTR were amplified using primer
492 pairs P11-P12 and P13-P14, respectively, and the sequence of mNeonGreen was
493 amplified using primers P15 and P16. Amplicons were then inserted into pKD[57] digested
494 with AatII and AscI. For expression of PfGAPM1 gRNA, oligo p20 was inserted into cut
495 PUF1-Cas9.

496 ## Parasite culture and transfections

497 *Plasmodium* parasites were cultured in RPMI 1640 medium (NF54^{attB}, VAC^{apt} and
498 GAPM1$^{mNG-apt}$) or in biotin-free medium (SBP1^{TbID}, VAC^{apt}/SBP1^{TbID}) [68] supplemented
499 with AlbuMAX I (Gibco), and transfected as described earlier[69].

500 For generation of SBP1^{TbID} parasites, a mix of two plasmids (50 µg each) were
501 transfected into NF54^{attB} parasites in duplicate. The plasmid mix contained the plasmid
502 pUF1-Cas9-SBP1gRNA, which contains the DHOD resistance gene, and the marker-
503 free plasmid pTOPO-SBP1-TbID. Drug pressure was applied 48 h after transfection,
504 using 1µM DSM1 [70] and selecting for Cas9 expression. After parasites grew back from
505 transfection, integration was confirmed by PCR, and then cloned using limiting dilution.
506 After clonal selection, cultures were transferred to biotin-free medium without DSM1.

507 For generation of VAC^{apt} and GAPM1$^{mNG-apt}$ parasites, the pKD-VAC-Apt and pKD-
508 GAPM1-mNG-Apt plasmids (20 µg) and the respective pUF1-Cas9 plasmid (50 µg)
509 were transfected into NF54^{attB} parasites in duplicate. Before transfection pKD plasmids
510 were digested overnight with EcoRV (NEB). The enzyme was then subjected to heat
511 inactivation for 20 min at 65 °C and then mixed with the pUF1-Cas9 plasmid.
512 Transfected parasites were grown in 0.5 µM anhydrous tetracycline (aTc) (Cayman
513 Chemical). Drug pressure was applied 48 h after transfection, using blasticidin (BSD) at
514 a concentration of 2.5 µg/mL, selecting for pKD-VAC-Apt and pKD-GAPM1-mNG-Apt
515 expression. After parasites grew back from transfection, integration was confirmed by
516 PCR, and then cloned using limiting dilution. Clones were maintained in mediums
517 containing 0.5 µM aTc and 2.5 µg/mL BSD.

518 For generation of VAC^{apt}/SBP1^{TbID} parasites, a mix of two plasmids: pTOPO-SBP1-TbID
519 and pUF1-Cas9-SBP1gRNA, was transfected into VAC^{apt} parasites. Drug pressure was
520 applied 48 h after transfection, using 1µM DSM1 [70] and selecting for Cas9 expression.
521 After parasites grew back from transfection, integration was confirmed by PCR, and
522 then cloned using limiting dilution.

523 ## Growth assays

524 For all assays, aliquots of parasite cultures were incubated in 8 μM Hoechst 33342
525 (ThermoFisher Scientific) for 20 min at room temperature and then fluorescence was
526 measured using a CytoFlex S (Beckman Coulter) flow-cytometer. Flow cytometry data
527 were analyzed using FlowJo software (Tree Star, Inc.) and plotted using Prism
528 (GraphPad Software, Inc.).

529 For the SBP1^{TbID} growth assay, asynchronous parasites were transferred to a 96-well
530 plate at 0.5% parasitemia and grown for 4 days. Parasitemia was monitored every 24 h.

531 For the VAC^{apt} and GAPM1$^{mNG\text{-}apt}$ growth assays, synchronous ring-stage parasites
532 were washed 5 times with RPMI 1640 medium and split into two cultures, one
533 resuspended in medium containing 0.5 μM aTc and 2.5 μg/mL BSD, and the other one
534 in medium containing only 2.5 μg/mL BSD. Then cultures were transferred to a 96-well
535 plate at 0.2% parasitemia and grown for 6 days. Parasitemia was monitored every 48 h.

536 ## Western blotting

537 For SBP1^{TbID} parasites, RIPA buffer (150 mM NaCl, 20mM Tris-HCl pH 7.5, 1mM
538 EDTA, 1% SDS, 0.1% Triton X-100) and sonication were used to disrupt parasite pellets
539 conserving all exported proteins. Briefly, late-stage parasites were isolated using a
540 Percoll gradient (Genesee Scientific). Pellets were then resuspended in RIPA buffer and
541 sonicated 3 times at 20% amplitude for 20 s. Protein supernatants were subsequently
542 solubilized in protein loading dye with Beta-mercaptoethanol (LI-COR Biosciences) and
543 used for SDS-PAGE.

544 For VAC^{apt} and GAPM1$^{mNG\text{-}apt}$ parasites, ice-cold 0.04% saponin in 1x PBS was used to
545 isolate parasites from host cells. Parasite pellets were subsequently solubilized in
546 protein loading dye with Beta-mercaptoethanol (LI-COR Biosciences) and used for
547 SDS-PAGE.

548 Primary antibodies used in this study were mouse-anti-V5 (Cell Signaling Technology,
549 1:1000), rabbit-anti-PfEF1α (from D. Goldberg, 1:2000), and mouse-anti-HA 6E2 (Cell

550 Signaling Technology, 1:2000). Secondary antibodies used were IRDye 680 CW goat-
551 anti-rabbit IgG, IRDye 800CW goat-anti-mouse IgG, and IRDye 800CW Streptavidin (Li-
552 COR Biosciences, 1:20 000 and 1:10 000). Membranes were imaged using the
553 Odyssey Clx Li-COR infrared imaging system (Li-COR Biosciences). Images were
554 processed and analyzed using ImageStudio (Li-COR Biosciences).

555 Immunofluorescence microscopy

556 For IFAs, cells were fixed as described previously [67]. The cell lines SBP1^{TbID} and
557 GAPM1^{apt} were smeared on a slide and fixed with acetone. The cell lines VAC^{apt} and
558 VAC^{apt}/SBP1^{TbID} were fixed with 4% paraformaldehyde (Electron Microscopy Sciences)
559 and 0.03% glutaraldehyde. Primary antibodies used were mouse-anti-V5 TCM5
560 (eBioscience, 1:100), rabbit-anti-V5 D3H8Q (Cell Signaling technology, 1:100), rabbit-
561 anti-HA 71550 (ThermoFisher Scientific, 1:100), rabbit-anti-MAHRP (from H. Beck,
562 1:500), mouse-anti-EXP2 7.7 and mouse-anti-KAHRP (from D. Cavanagh; 1:1000,
563 1:500 respectively). Secondary antibodies used were Alexa Fluor 488, Alexa Fluor 546,
564 and Streptavidin Alexa Fluor 488 (Life Technologies, 1:1000). Cells were mounted using
565 ProLong Diamond with 4',6'-diamidino-2-phenylindole (DAPI) (Invitrogen) and imaged
566 using a DeltaVision II microscope system with an Olympus Ix-71 inverted microscope.
567 Images were collected as a Z-stack and deconvolved using SoftWorx, then displayed as
568 a maximum intensity projection. Adjustments to brightness and contrast were made for
569 display purposes using Adobe Photoshop.

570 Synchronization assays

571 For detection of SBP1 during export, SBP1^{TbID} parasites were synchronized with two
572 series of 5% sorbitol treatment. Then, schizont-stage parasites were isolated using
573 Percoll gradient (Genesee Scientific) and immediately transferred to previously warmed
574 fresh red blood cells at 1% hematocrit. Parasites were allowed to egress and invade
575 new red blood cells, and samples were obtained for IFAs at different time points.

576 ## SBP1^{TbID} proximity biotinylation and mass spectrometry

577 Biotinylation by TbID-tagged SBP1 was confirmed by collecting SBP1^{TbID} parasites for
578 Western blotting and IFAs after incubation for 2 h in biotin-free media supplemented
579 with 50 μM biotin.

580 For detection of SBP1 during export, SBP1^{TbID} parasites were synchronized with two
581 series of 5% sorbitol treatment. Then, late-schizont-stage parasites were isolated using
582 a Percoll gradient (Genesee Scientific). Parasites were then split in two, and
583 immediately transferred to red blood cells at 1% hematocrit in warm medium without or
584 with biotin (50 μM). Both parasite cultures were incubated for 4 h at 37°C with shaking
585 to let them egress and invade new red blood cells. Cultures were then treated with 5%
586 sorbitol to remove remaining late-stage parasites. Biotinylated culture was washed in 1X
587 PBS, incubated on ice for 10 min to inactivate biotinylation and then stored at -80 °C,
588 until processing. Non-biotinylated culture was incubated for 16 h at 37°C with shaking,
589 then incubated for 4 h in medium with biotin and finally collected as previously
590 described.

591 Parasite pellets were lysed using extraction buffer (40 mM Tris-HCL pH 7.6, 150 mM
592 KCl, 1mM EDTA, 5% NP-40 and 1X HALT) and sonication (3x, 10% amplitude, 20 s
593 pulses). Streptavidin MagneSphere Paramagnetic Particle beads (Promega) were used
594 to isolate biotinylated proteins. Beads were washed three times in 1 mL of 1X PBS.
595 Protein lysates were incubated with the Streptavidin beads for 1 h at room temperature.
596 After removal of the unbound fraction, the magnetic beads were washed twice with an
597 extraction buffer and once in 1X PBS. The biotinylated proteins on the magnetic beads
598 were digested and analyzed at the Proteomics and Metabolomics shared resource at
599 Fred Hutchinson Cancer Research Center using a Orbitrap Fusion with ETD Mass
600 Spectrometer. All proteins identified in this study are in Supplemental Table 2. All mass
601 spectrometry proteomic data have been deposited to the ProteomeXchange consortium
602 via the MassIVE partner repository with the dataset identified PXD034946 (Project
603 name: Rapid proximity biotinylation of the *Plasmodium falciparum* exported protein,
604 SBP1).

605 ## REFERENCES

606 1. World Health Organization & Others. World malaria report 2021. (2021).

607 2. Moxon, C. A., Gibbins, M. P., McGuinness, D., Milner, D. A., Jr & Marti, M. New Insights
608 into Malaria Pathogenesis. *Annu. Rev. Pathol.* **15**, 315–343 (2020).

609 3. Ashley, E. A., Pyae Phyo, A. & Woodrow, C. J. Malaria. *Lancet* **391**, 1608–1621 (2018).

610 4. Spillman, N. J., Beck, J. R. & Goldberg, D. E. Protein export into malaria parasite-infected
611 erythrocytes: mechanisms and functional consequences. *Annu. Rev. Biochem.* **84**, 813–
612 841 (2015).

613 5. Spielmann, T. & Gilberger, T. W. Critical Steps in Protein Export of Plasmodium falciparum
614 Blood Stages. *Trends Parasitol.* **31**, 514–525 (2015).

615 6. Matthews, K. M., Pitman, E. L. & de Koning-Ward, T. F. Illuminating how malaria parasites
616 export proteins into host erythrocytes. *Cell. Microbiol.* **21**, e13009 (2019).

617 7. de Koning-Ward, T. F., Dixon, M. W. A., Tilley, L. & Gilson, P. R. Plasmodium species:
618 master renovators of their host cells. *Nat. Rev. Microbiol.* **14**, 494–507 (2016).

619 8. Maier, A. G., Cooke, B. M., Cowman, A. F. & Tilley, L. Malaria parasite proteins that
620 remodel the host erythrocyte. *Nat. Rev. Microbiol.* **7**, 341–354 (2009).

621 9. Desai, S. A. Why do malaria parasites increase host erythrocyte permeability? *Trends*
622 *Parasitol.* **30**, 151–159 (2014).

623 10. Hiller, N. L. *et al.* A host-targeting signal in virulence proteins reveals a secretome in
624 malarial infection. *Science* **306**, 1934–1937 (2004).

625 11. Marti, M., Good, R. T., Rug, M., Knuepfer, E. & Cowman, A. F. Targeting malaria virulence
626 and remodeling proteins to the host erythrocyte. *Science* **306**, 1930–1933 (2004).

627 12. Heiber, A. *et al.* Identification of new PNEPs indicates a substantial non-PEXEL exportome
628 and underpins common features in Plasmodium falciparum protein export. *PLoS Pathog.* **9**,
629 e1003546 (2013).

630 13. Blisnick, T. *et al.* Pfsbp1, a Maurer's cleft Plasmodium falciparum protein, is associated with
631 the erythrocyte skeleton. *Mol. Biochem. Parasitol.* **111**, 107–121 (2000).
632 14. Saridaki, T., Frohlich, K. S., Braun-Breton, C. & Lanzer, M. Export of PfSBP1 to the
633 Plasmodium falciparum Maurer's clefts. *Traffic* **10**, 137–152 (2009).
634 15. Maier, A. G. *et al.* Skeleton-binding protein 1 functions at the parasitophorous vacuole
635 membrane to traffic PfEMP1 to the Plasmodium falciparum-infected erythrocyte surface.
636 *Blood* **109**, 1289–1297 (2007).
637 16. Spycher, C. *et al.* MAHRP-1, a novel Plasmodium falciparum histidine-rich protein, binds
638 ferriprotoporphyrin IX and localizes to the Maurer's clefts. *J. Biol. Chem.* **278**, 35373–35383
639 (2003).
640 17. Spycher, C. *et al.* The Maurer's cleft protein MAHRP1 is essential for trafficking of PfEMP1
641 to the surface of Plasmodium falciparum-infected erythrocytes. *Mol. Microbiol.* **68**, 1300–
642 1314 (2008).
643 18. Su, X. Z. *et al.* The large diverse gene family var encodes proteins involved in
644 cytoadherence and antigenic variation of Plasmodium falciparum-infected erythrocytes. *Cell*
645 **82**, 89–100 (1995).
646 19. Baruch, D. I. *et al.* Cloning the P. falciparum gene encoding PfEMP1, a malarial variant
647 antigen and adherence receptor on the surface of parasitized human erythrocytes. *Cell* **82**,
648 77–87 (1995).
649 20. Baruch, D. I. *et al.* Identification of a region of PfEMP1 that mediates adherence of
650 Plasmodium falciparum infected erythrocytes to CD36: conserved function with variant
651 sequence. *Blood* **90**, 3766–3775 (1997).
652 21. Spielmann, T. *et al.* A cluster of ring stage-specific genes linked to a locus implicated in
653 cytoadherence in Plasmodium falciparum codes for PEXEL-negative and PEXEL-positive
654 proteins exported into the host cell. *Mol. Biol. Cell* **17**, 3613–3624 (2006).

655 22. Gruring, C. *et al.* Uncovering common principles in protein export of malaria parasites. *Cell*
656 *Host Microbe* **12**, 717–729 (2012).
657 23. Beck, J. R., Muralidharan, V., Oksman, A. & Goldberg, D. E. PTEX component HSP101
658 mediates export of diverse malaria effectors into host erythrocytes. *Nature* **511**, 592–595
659 (2014).
660 24. Elsworth, B. *et al.* PTEX is an essential nexus for protein export in malaria parasites.
661 *Nature* **511**, 587–591 (2014).
662 25. Beck, J. R. & Ho, C. M. Transport mechanisms at the malaria parasite-host cell interface.
663 *PLoS Pathog.* **17**, e1009394 (2021).
664 26. Garten, M. & Beck, J. R. Structured to conquer: transport across the Plasmodium
665 parasitophorous vacuole. *Curr. Opin. Microbiol.* **63**, 181–188 (2021).
666 27. Matthews, K. M., Kalanon, M. & de Koning-Ward, T. F. Uncoupling the Threading and
667 Unfoldase Actions of Plasmodium HSP101 Reveals Differences in Export between Soluble
668 and Insoluble Proteins. *MBio* **10**, (2019).
669 28. Gabriela, M. *et al.* A revised mechanism for how Plasmodium falciparum recruits and
670 exports proteins into its erythrocytic host cell. *PLoS Pathog.* **18**, e1009977 (2022).
671 29. Batinovic, S. *et al.* An exported protein-interacting complex involved in the trafficking of
672 virulence determinants in Plasmodium-infected erythrocytes. *Nat. Commun.* **8**, 16044
673 (2017).
674 30. Jonsdottir, T. K. *et al.* Characterisation of complexes formed by parasite proteins exported
675 into the host cell compartment of Plasmodium falciparum infected red blood cells. *Cell.*
676 *Microbiol.* **23**, e13332 (2021).
677 31. Carmo, O. M. S. *et al.* Virulence determinant, PTP7, controls vesicle budding from the
678 Maurer's clefts, adhesin protein trafficking and host cell remodeling in Plasmodium
679 falciparum. *bioRxiv* 2021.08.12.456062 (2021) doi:10.1101/2021.08.12.456062.
680 32. Takano, R. *et al.* A High-Resolution Map of SBP1 Interactomes in Plasmodium falciparum-

681 infected Erythrocytes. *iScience* **19**, 703–714 (2019).
682 33. McHugh, E. *et al.* Role of Plasmodium falciparumProtein GEXP07 in Maurer's Cleft
683 Morphology, Knob Architecture, and P. falciparumEMP1 Trafficking. *MBio* **11**, 479 (2020).
684 34. Branon, T. C. *et al.* Efficient proximity labeling in living cells and organisms with TurboID.
685 *Nat. Biotechnol.* **36**, 880–887 (2018).
686 35. May, D. G., Scott, K. L., Campos, A. R. & Roux, K. J. Comparative Application of BioID and
687 TurboID for Protein-Proximity Biotinylation. *Cells* **9**, (2020).
688 36. Nkrumah, L. J. *et al.* Efficient site-specific integration in Plasmodium falciparum
689 chromosomes mediated by mycobacteriophage Bxb1 integrase. *Nat. Methods* **3**, 615–621
690 (2006).
691 37. Mundwiler-Pachlatko, E. & Beck, H.-P. Maurer's clefts, the enigma of Plasmodium
692 falciparum. *Proc. Natl. Acad. Sci. U. S. A.* **110**, 19987–19994 (2013).
693 38. Cooke, B. M. *et al.* A Maurer's cleft-associated protein is essential for expression of the
694 major malaria virulence antigen on the surface of infected red blood cells. *J. Cell Biol.* **172**,
695 899–908 (2006).
696 39. Iriko, H. *et al.* Skeleton binding protein 1 (SBP1) of Plasmodium falciparum accumulates in
697 electron-dense material before passing through the parasitophorous vacuole membrane.
698 *Parasitol. Int.* **75**, 102003 (2020).
699 40. Dellibovi-Ragheb, T. A. *et al.* Host biotin is required for liver stage development in malaria
700 parasites. *Proceedings of the National Academy of Sciences* **115**, E2604–E2613 (2018).
701 41. Larochelle, M., Bergeron, D., Arcand, B. & Bachand, F. Proximity-dependent biotinylation
702 mediated by TurboID to identify protein-protein interaction networks in yeast. *J. Cell Sci.*
703 **132**, (2019).
704 42. Roux, K. J., Kim, D. I., Raida, M. & Burke, B. A promiscuous biotin ligase fusion protein
705 identifies proximal and interacting proteins in mammalian cells. *J. Cell Biol.* **196**, 801–810
706 (2012).

707 43. Kim, D. I. *et al.* An improved smaller biotin ligase for BioID proximity labeling. *Mol. Biol. Cell*
708 **27**, 1188–1196 (2016).
709 44. Kudyba, H. M. *et al.* The endoplasmic reticulum chaperone PfGRP170 is essential for
710 asexual development and is linked to stress response in malaria parasites. *Cell. Microbiol.*
711 **21**, e13042 (2019).
712 45. Ho, C.-M. *et al.* Malaria parasite translocon structure and mechanism of effector export.
713 *Nature* **19**, 1 (2018).
714 46. Garten, M. *et al.* EXP2 is a nutrient-permeable channel in the vacuolar membrane of
715 Plasmodium and is essential for protein export via PTEX. *Nat Microbiol* **3**, 1090–1098
716 (2018).
717 47. Charnaud, S. C., Kumarasingha, R., Bullen, H. E., Crabb, B. S. & Gilson, P. R. Knockdown
718 of the translocon protein EXP2 in Plasmodium falciparum reduces growth and protein
719 export. *PLoS One* **13**, e0204785 (2018).
720 48. Grüring, C. *et al.* Development and host cell modifications of Plasmodium falciparum blood
721 stages in four dimensions. *Nat. Commun.* **2**, 165 (2011).
722 49. McMillan, P. J. *et al.* Spatial and temporal mapping of the PfEMP1 export pathway in
723 Plasmodium falciparum. *Cell. Microbiol.* **15**, 1401–1418 (2013).
724 50. Lobingier, B. T. *et al.* An Approach to Spatiotemporally Resolve Protein Interaction
725 Networks in Living Cells. *Cell* **169**, 350–360.e12 (2017).
726 51. Mair, A., Xu, S.-L., Branon, T. C., Ting, A. Y. & Bergmann, D. C. Proximity labeling of
727 protein complexes and cell-type-specific organellar proteomes in Arabidopsis enabled by
728 TurboID. *Elife* **8**, (2019).
729 52. Santos-Barriopedro, I., van Mierlo, G. & Vermeulen, M. Off-the-shelf proximity biotinylation
730 for interaction proteomics. *Nat. Commun.* **12**, 5015 (2021).
731 53. Amos, B. *et al.* VEuPathDB: the eukaryotic pathogen, vector and host bioinformatics
732 resource center. *Nucleic Acids Res.* **50**, D898–D911 (2022).

733 54. Kono, M., Prusty, D., Parkinson, J. & Gilberger, T. W. The apicomplexan inner membrane
734 complex. *Front. Biosci.* **18**, 982–992 (2013).
735 55. Kono, M. *et al.* Evolution and architecture of the inner membrane complex in asexual and
736 sexual stages of the malaria parasite. *Mol. Biol. Evol.* **29**, 2113–2132 (2012).
737 56. Bullen, H. E. *et al.* A Novel Family of Apicomplexan Glideosome-associated Proteins with
738 an Inner Membrane-anchoring Role. *Journal of Biological Chemistry* vol. 284 25353–25363
739 (2009).
740 57. Rajaram, K., Liu, H. B. & Prigge, S. T. Redesigned TetR-Aptamer System To Control Gene
741 Expression in Plasmodium falciparum. *mSphere* **5**, (2020).
742 58. de Koning-Ward, T. F. *et al.* A newly discovered protein export machine in malaria
743 parasites. *Nature* **459**, 945–949 (2009).
744 59. Maier, A. G. *et al.* Exported proteins required for virulence and rigidity of Plasmodium
745 falciparum-infected human erythrocytes. *Cell* **134**, 48–61 (2008).
746 60. Vincensini, L. *et al.* Proteomic analysis identifies novel proteins of the Maurer's clefts, a
747 secretory compartment delivering Plasmodium falciparum proteins to the surface of its host
748 cell. *Mol. Cell. Proteomics* **4**, 582–593 (2005).
749 61. Das, S., Basu, H., Korde, R., Tewari, R. & Sharma, S. Arrest of nuclear division in
750 Plasmodium through blockage of erythrocyte surface exposed ribosomal protein P2. *PLoS*
751 *Pathog.* **8**, e1002858 (2012).
752 62. Muralidharan, V., Oksman, A., Pal, P., Lindquist, S. & Goldberg, D. E. Plasmodium
753 falciparum heat shock protein 110 stabilizes the asparagine repeat-rich parasite proteome
754 during malarial fevers. *Nat. Commun.* **3**, 1310 (2012).
755 63. Birnbaum, J. *et al.* A genetic system to study Plasmodium falciparum protein function. *Nat.*
756 *Methods* **14**, 450–456 (2017).
757 64. Araiso, Y., Imai, K. & Endo, T. Role of the TOM Complex in Protein Import into
758 Mitochondria: Structural Views. *Annu. Rev. Biochem.* **91**, 679–703 (2022).

759 65. Lamb, I. M. *et al.* Mitochondrially targeted proximity biotinylation and proteomic analysis in
760 Plasmodium falciparum. *bioRxiv* 2022.05.30.494025 (2022)
761 doi:10.1101/2022.05.30.494025.
762 66. Claros, M. G. & Vincens, P. Computational method to predict mitochondrially imported
763 proteins and their targeting sequences. *Eur. J. Biochem.* **241**, 779–786 (1996).
764 67. Cobb, D. W. *et al.* The Exported Chaperone PfHsp70x Is Dispensable for the Plasmodium
765 falciparum Intraerythrocytic Life Cycle. *mSphere* **2**, e00363–17 (2017).
766 68. Zimbres, F. M. *et al.* Metabolomics profiling reveals new aspects of dolichol biosynthesis in
767 Plasmodium falciparum. *Sci. Rep.* **10**, 401 (2020).
768 69. Kudyba, H. M., Cobb, D. W., Florentin, A., Krakowiak, M. & Muralidharan, V. CRISPR/Cas9
769 Gene Editing to Make Conditional Mutants of Human Malaria Parasite P. falciparum. *J. Vis.*
770 *Exp.* 1–10 (2018).
771 70. Ganesan, S. M. *et al.* Yeast dihydroorotate dehydrogenase as a new selectable marker for
772 Plasmodium falciparum transfection. *Mol. Biochem. Parasitol.* **177**, 29–34 (2011).

773
774
775
776
777
778
779
780
781
782
783
784
785

786 **SUPPLEMENTAL FIGURES**

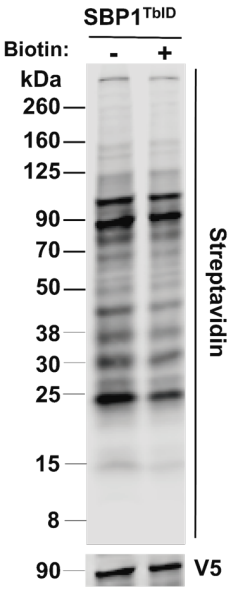

787

788 **Supplemental figure 1. Biotinylation of proximal proteins by TurboID$_{V5}$-tagged SBP1**.
789 Western blot of parasite lysates isolated from the mutant line SBP1^{TbID} grown in complete RPMI
790 medium, incubated with or without biotin (50 μM) for 2 h. Samples were probed with antibodies
791 against V5 (loading control) and fluorescent dye-labeled streptavidin. The protein marker sizes
792 are shown on the left.

793

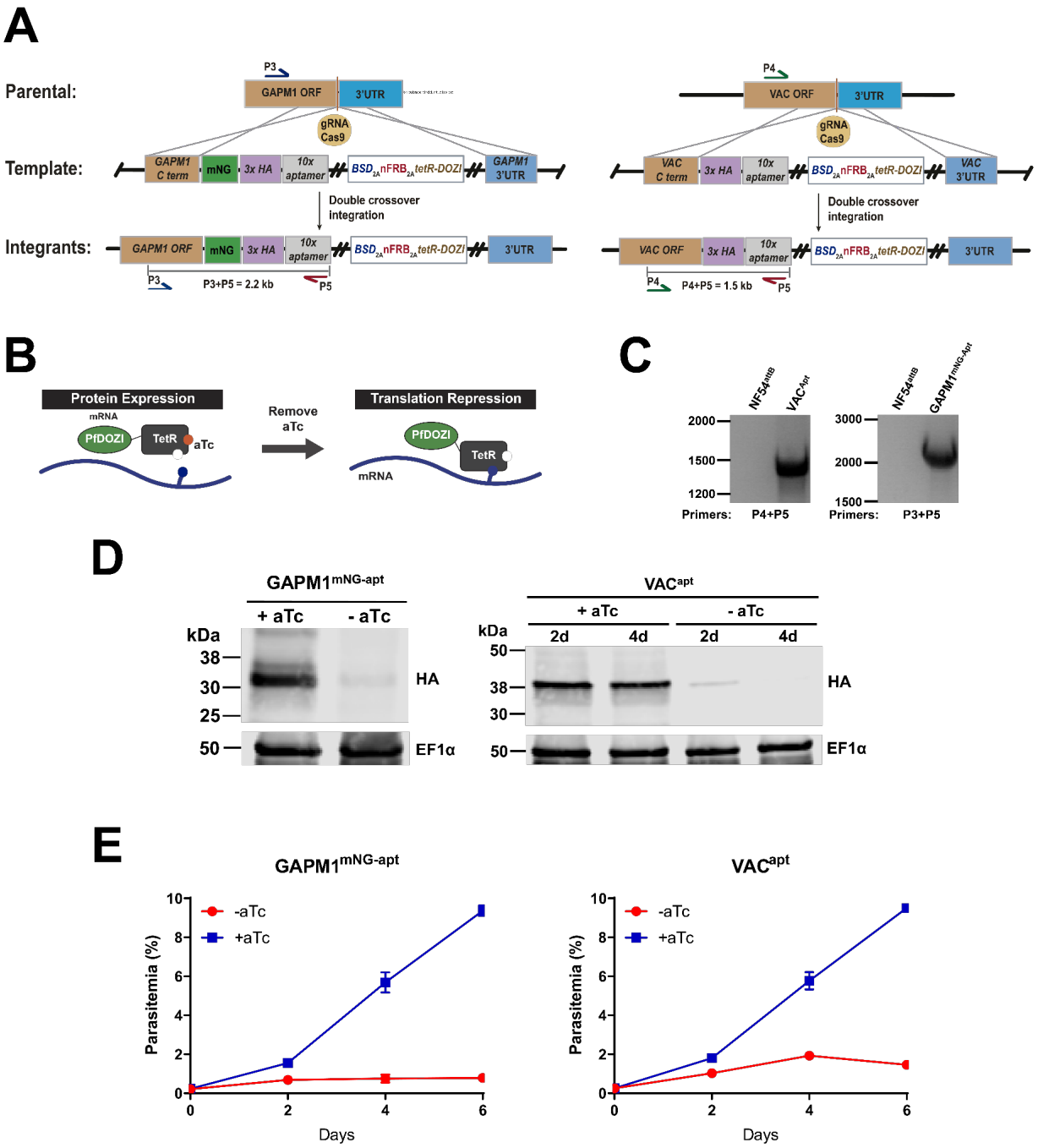

Supplemental figure 2. Characterization of parasite lines VAC^{apt} and GAPM1$^{mNG\text{-}apt}$. (A) Schematic showing the integration of the repair plasmid to modify the genomic loci of Pf3D7_1432100 (VAC) and Pf3D7_1323700 (GAPM1). Cas9 introduces a double-stranded break at the C-terminus of the VAC and GAPM1 locus. The repair plasmid provides homology regions for double-crossover homologous recombination, introducing the HA-tag and the TetR-Aptamer system. For GAPM1$^{mNG\text{-}apt}$, a fluorescent tag mNeonGreen was introduced between the C-terminus and the HA-tag. (B) Regulation of protein expression using the TetR-Aptamer knockdown system. TetR binds to aptamer repeats in the mRNA, while PfDOZI localizes the

complex to sites of mRNA sequestration, causing a repression in translation of the gene of interest. Anhydrous tetracycline (aTc) binds to TetR, blocking its interaction with the aptamers. (C) PCR test confirming integration at the VAC and GAPM1 locus. Amplicons were amplified from genomic DNA isolated from mutant and wild-type parasites. Primers were designed to amplify the region between the C-terminus and the tandem of 10X aptamer repeats. (D) Western blot of parasite lysates isolated from the mutant lines VAC^{apt} and GAPM1$^{mNG\text{-}apt}$ probed with antibodies against HA and EF1α (loading control). The protein marker sizes are shown on the left. GAPM1$^{mNG\text{-}apt}$ parasites were collected after incubation for 48 h in the presence or absence of aTc. VAC^{apt} parasites were collected after incubation for 48 and 96 h in presence or absence of aTc. (E) Growth of synchronous VAC^{apt} and GAPM1$^{mNG\text{-}apt}$ parasites over 6 days after removal of aTc from the medium via flow cytometry. Representative of three biological replicates shown for each growth curve. Each data point represents the mean of three technical replicates; error bars represent standard deviation.

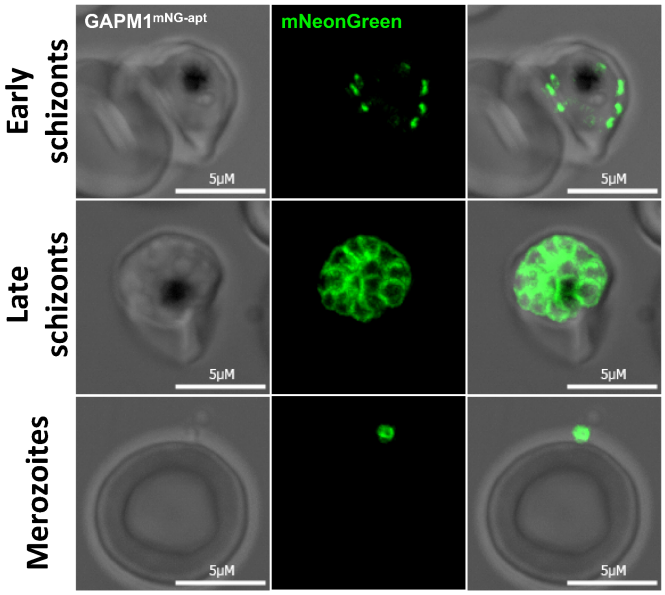

Supplemental figure 3. Localization of GAPM1 at late stages in the GAPM1$^{mNG\text{-}apt}$ cell line. (A) Representative live images showing GAPM1$^{mNG\text{-}apt}$ localization at early and late schizonts, and merozoites. Images of GAPM1$^{mNG\text{-}apt}$ from left to right are phase-contrast, mNeonGreen (green), and fluorescence merge. Z stack images were deconvolved and projected as a combined single image.

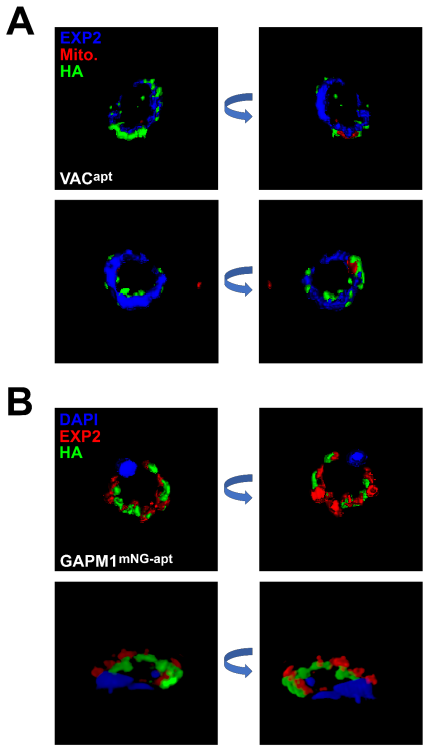

829

830 **Supplemental figure 4. Localization of VAC and GAPM1 at early stage parasites.** 3D
831 reconstruction based on structured illumination microscopy images captured from (A) VAC^{apt}
832 and (B) GAPM1$^{mNG\text{-}apt}$ ring-stage parasites at 4 hpi and stained with the antibodies as in Fig 5A.

833
834
835
836
837
838
839 **Supplemental Table 1.** List of primers used in the study to generate the cell lines SBP1^{TbID},
840 VAC^{apt} and GAPM1$^{mNG\text{-}apt}$
841
842
843 **Supplemental Table 2.** Complete list of proteins identified using label-free analysis and
844 collected by mass spectrometry.